

Article

A Novel Generalized Clapeyron Equation-Based Model for Capturing the Soil Freezing Characteristics Curve of Saline Soil: Validation by Small Sample Lab and Field Experiments

Liwen Wang ¹, Xianghao Wang ^{1,2}, Juan Han ^{1,3}, Chaozi Wang ^{1,*}, Chenglong Zhang ¹ and Zailin Huo ^{1,*}

¹ Center for Agricultural Water Research in China, China Agricultural University, Beijing 100083, China; cauwangliwen@163.com (L.W.); xianghaowang@126.com (X.W.); hanjuan2024@163.com (J.H.); zhangcl1992@cau.edu.cn (C.Z.)

² College of Water Conservancy & Civil Engineering, Northeast Agricultural University, Harbin 150030, China

³ Department of Geology and Surveying and Mapping, Shanxi Institute of Energy, Jinzhong 030600, China

* Correspondence: chaoziwang@cau.edu.cn (C.W.); huozi@cau.edu.cn (Z.H.); Tel.: +86-185-1000-6639 (C.W.)

Abstract: The soil freezing characteristic curve (SFCC) describes the relationship between the freezing point and unfrozen water content, which are two critical parameters in depicting the heat, solute, and water transport in frozen soil. In this paper, we propose a novel Generalized Clapeyron Equation (GCE)-based model, the GCE-Salt Model, to better capture the SFCC in frozen soil in the presence of solute. It keeps the matric potential Ψ_f in the GCE as its original meaning and incorporates the effect of solute potential in the equilibrium freezing temperature. The performance of our GCE-Salt Model was validated by both lab and field experimental data and compared with related models (Combined Model and GCE-Tan Model). The GCE-Salt Model performed exceptionally well in extremely saline soil and it performed well in both non-saline and saline soil. (1) Our GCE-Salt Model could capture the SFCC of non-saline soil equally as well as the Combined Model (NSE = 0.866); (2) our GCE-Salt Model performed similarly well as the Combined Model and a little better than the GCE-Tan Model for the slightly to highly saline soil (NSE \geq 0.80 for three models); and (3) our GCE-Salt Model (NSE = 0.919) beat the Combined Model (NSE = 0.863) and the GCE-Tan Model (NSE = 0.62) in capturing the SFCC of extremely saline soil, mainly because the inherent expression of our GCE-Salt Model can more accurately capture the freezing point. Our findings highlight the effect of solute potential on the ice–water change and could improve the understanding of the effect of freezing and thawing on the thermal–hydrological processes, structure of saline soil, and landscape evolution in cold regions.

Keywords: saline soil; the soil freezing characteristic curve; prediction model; freezing processes; solute potential; small sample experiment



Citation: Wang, L.; Wang, X.; Han, J.; Wang, C.; Zhang, C.; Huo, Z. A Novel Generalized Clapeyron Equation-Based Model for Capturing the Soil Freezing Characteristics Curve of Saline Soil: Validation by Small Sample Lab and Field Experiments. *Water* **2024**, *16*, 670. <https://doi.org/10.3390/w16050670>

Academic Editor: Maria Antonia López-Antón

Received: 16 January 2024

Revised: 14 February 2024

Accepted: 17 February 2024

Published: 25 February 2024



Copyright: © 2024 by the authors. Licensee MDPI, Basel, Switzerland. This article is an open access article distributed under the terms and conditions of the Creative Commons Attribution (CC BY) license (<https://creativecommons.org/licenses/by/4.0/>).

1. Introduction

Understanding soil freezing and thawing is vital in understanding winter evapotranspiration [1], runoff [2], groundwater recharge periodically [3], soil formation [4], predicting the movement of nutrients/contaminants as they seep through frozen layers of soil [5], and landscape evolution [6] in cold regions. The soil pores were expanded by soil frost heaving during the freezing period [7–9]. Whereas, the soil pore collapsed along with the ice–water phase change during thawing [4,10,11]. As the soil pore expansion was dominant, after a seasonal freezing–thawing cycle, the soil was less compacted [10] and its porosity increased [4,10]. What is more, the presence of salt will further complicate the influence of freezing and thawing on soil structure and landscape evolution [6]. Therefore, this study focuses on the freezing process of saline soil, which is prevalent in the middle and high latitudes of Asia [12–15], Europe [16,17], and America [1,12]. However, characterizing the

ice–water phase change in saline soil is still challenging due to the complicated interaction between the soil matric potential and the solute potential [13,14].

The soil freezing characteristic curve (SFCC) describes the equilibrium state of the ice–water phase change [15] by illustrating the decline in the liquid volume ratio in the pore space as temperature decreases during the ice–water phase change [16]. As summarized by Bi et al. [17], the models described by the SFCC can be categorized into four types: the theoretical models [18–20], the SWCC-based models [12,21–25], the empirical models [26–37], and the estimation models [31,38,39]. However, only a few SFCC models have considered the presence of salt or solute [1,14,40–46]. Wu et al. [14] proposed an improved empirical model by substituting the freezing point of the SFCC model proposed by Xu et al. [47] with the freezing point of the salt solution according to Banin and Anderson [48]. The empirical models could well capture the experimental soils [27] but might be hard to apply to soils of other types [17]. For the theoretical models [43,44], Wang et al. [43] proposed a phase composition model based on the assumption that soil particles are spheres and the unfrozen water covers the spherical soil particles as a thin film. Wan and Yang [44] built a theoretical model considering the soil pore size distribution and the effect of ion concentrations. The theoretical models have gained prominence in recent years [39] because they have clear physical meanings which are based on the pore size distribution of soil [17,18,44,49] or the surface effects of soil particles [18,43,50,51]. However, theoretical models usually possess complicated equations [18–20,50].

Whereas, the SWCC-based models integrate the Clapeyron equation with the soil water characteristic curve (SWCC) [12,52–56] based on the similarity of SFCC and SWCC [39] and take advantage of soil hydraulic parameters. Thus, once the soil hydraulic parameters are obtained for a soil, its SFCC could be readily obtained via SWCC-based models. In recent years, some SWCC-based SFCC models have been developed for saline soils. Except for Zhou et al. [42], whose model was based on the Brooks and Corey model [57], most of the existing SWCC-based SFCC models are based on the van Genuchten model. Under low salinity conditions (<1.0% g/g dry soil), Tan et al. [46] proposed an improved GCE model, which excluded the osmotic potential from the total soil water potential [58] in the SWCC before using GCE to predict SFCCs. Wan et al. [59] improved the van Genuchten model-based SFCC model by considering the effect of salt concentration on the ice nucleation and on the freezing point. Amankwah et al. [1] proposed a Combined Model, combining the GCE and a newly developed Salt Exclusion model, to well capture the SFCC of both non-saline and saline soil. However, most of these models are not easily used in actual areas and are still limited to the theoretical level or laboratory. The Combined Model proposed by Amankwah has a clear physical meaning and is handy in application. We found that the salt concentration in the experimental area of this research is smaller than that in our area. There is a lack of modeling under a wider range of salt concentrations.

Based on the GCE, the fundamental improvement in the Combined Model is the (1) expression of the equilibrium freezing temperature T_f as $T_d + T_0$ to consider the effect of soil matric potential and (2) replacement of the freezing initiation temperature T_0 in the denominator by T_m to consider the effect of solute potential. That is to say, Amankwah et al. [1] regarded the Ψ_f as the summation of soil matric potential and solute potential but not the original soil matric potential any more. Alternatively, we could keep the Ψ_f as the soil matric potential and exclude the effect of solute potential in the numerator. Inspired by the expression of the freezing point by Wang et al. [43], we keep the T_0 in the denominator as the reference state and consider both the effect of soil matric potential and the effect of solute potential in the numerator, i.e., the equilibrium freezing temperature is $T_0 + \Delta T_{fm} = T_f - \Delta T_{fs}$.

The objective of this study is to propose a novel model that describes the SFCC considering the solute potential and test the ability of our newly proposed model to capture the ice–water phase change in frozen saline soil, especially, the ability to capture the freezing point of soil pore water at different salinity levels.

2. Materials and Methods

2.1. Modelling

2.1.1. The Combined Model

Amankwah et al. [1] proposed a Combined Model describing the SFCC by combining the conventional GCE model and a new Salt Exclusion Model, considering both the effect of capillary and adsorption and the effect of solute exclusion on the freezing point depression.

(1) The GCE

Based on the similarity between the SFCC and the SWCC, Amankwah et al. [1] adopted the van Genuchten equation [60] to describe the relationship between the liquid soil water potential and the liquid soil water content as follows:

$$\theta_l = \theta_r + (\theta_s - \theta_r)(1 + (\alpha\psi_l)^n)^{-m} \quad (1)$$

where θ_l is the volumetric unfrozen water content ($\text{cm}^3 \cdot \text{cm}^{-3}$), θ_r is the residual water content ($\text{cm}^3 \cdot \text{cm}^{-3}$), θ_s is the saturated soil water content ($\text{cm}^3 \cdot \text{cm}^{-3}$), Ψ_l (m) is the matric potential. α is the inverse of the air-entry value (m^{-1}), n is the pore-size distribution index, and $m = 1 - 1/n$. Amankwah et al. [1] proposed that the GCE can be expressed as

$$\psi_f = \frac{L}{g} \ln\left(\frac{T_f}{T_0}\right) = \frac{L}{g} \ln\left(\frac{T_d + T_0}{T_0}\right) \quad (2)$$

where Ψ_f (m) is soil matric potential, which predicts the liquid water content; T_f ($^{\circ}\text{C}$) is the equilibrium freezing temperature of soil water; L ($\text{J} \cdot \text{kg}^{-1}$) is the latent heat of fusion; g ($\text{m} \cdot \text{s}^{-2}$) is gravitational acceleration; and T_0 (K) is the freezing temperature for free pure water at atmospheric pressure 273.15 K (0°C). Particularly, Amankwah et al. [1] expressed the equilibrium freezing temperature T_f as $T_d + T_0$ to consider the effect of soil matric potential.

Then, Ψ_l can be expressed as

$$\psi_l = \begin{cases} \psi_u, & \psi_f \geq \psi_u \\ \frac{L}{g} \ln\left(\frac{T_d + T_0}{T_0}\right), & \psi_f < \psi_u \end{cases} \quad (3)$$

where Ψ_u (m) is the equivalent unfrozen matric potential.

Then, the GCE model can be expressed as

$$\theta_l = \theta_r + (\theta_s - \theta_r) \left(1 + \left(\alpha \frac{L_f}{g} \ln\left(\frac{T_d + T_0}{T_0}\right)\right)^n\right)^{-m}, \psi_f < \psi_u \quad (4)$$

(2) The Salt Exclusion Model

Then, Amankwah et al. [1] proposed a Salt Exclusion Model, describing the freezing point depression because of salt concentrate, considering the saline water concentrated due to the transition of liquid water to ice:

$$T_m = p_1 c^2 + p_2 c \quad (5)$$

where T_m is the minimum temperature below T_0 at which the saline water of a given concentration will freeze. $c = c_b / (\theta_l - \theta_r)$; c_b is the bulk solute concentration in the soil, i.e., the mass of salt per unit volume of soil. The p_1 and p_2 are fitted parameters obtained by the relationship between freezing point depression and salt concentration and the values of p_1 and p_2 were found to be -0.00012544 and -0.05561807 , respectively. Combining the relationship between c and θ_l and the relationship between T_m and c ,

Amankwah et al. [1] obtained the unfrozen water content for a given soil temperature in one bulk solute concentration as

$$\theta_l = \theta_r + \frac{2c_b p_1}{-p_2 - \sqrt{p_2^2 + 4p_1 T_d}} \tag{6}$$

(3) The Combined Model

Amankwah et al. [1] finally obtained the Combined Model by replacing the freezing initiation temperature T_0 in the denominator of Equation (4) with T_m (the freezing point considered solute potential) to consider both the effect of soil matric potential and the effect of solute potential on the freezing point depression as follows:

$$\theta_l = \theta_r + (\theta_s - \theta_r) \left(1 + \left(\alpha \frac{L_f}{g} \ln \left(\frac{T_d + T_0}{T_m} \right) \right)^n \right)^{-m} \tag{7}$$

2.1.2. The GCE-Salt Model

Equation (2) expresses the relationship between the matric potential Ψ_f and the equilibrium freezing temperature T_f (K). Comparing Equations (4) and (7), the fundamental improvement in the Combined Model based on the GCE is the (1) expression of the T_f as $T_d + T_0$ to consider the effect of capillary and adsorption and (2) replacement of the T_0 in the denominator by T_m to consider the effect of solute potential. That is to say, Amankwah et al. [1] regarded Ψ_f as the summation of soil matric potential and solute potential but not the original soil matric potential anymore.

Then, we happened to see that Wang et al. [43] express the freezing point T_f (K) as

$$T_f = T_0 + \Delta T_{fm} + \Delta T_{fs} \tag{8}$$

where ΔT_{fm} (K) is the freezing point depression induced by soil matric potential when salt concentration $c = 0$, the same as the T_d in the Equation (2), and ΔT_{fs} (K) is the freezing point depression induced by solute potential, the same as the T_m in the Equation (2).

Inspired by Equation (8), we, instead, keep the T_0 in the denominator as the reference state and consider both the effect of soil matric potential and the effect of solute potential in the numerator, i.e., the equilibrium freezing temperature is $T_0 + \Delta T_{fm} = T_f - \Delta T_{fs}$. In other words, we keep the Ψ_f as the soil matric potential and exclude the effect of solute potential in the numerator. Substituting $T_d = \Delta T_{fm}$ and $T_0 + \Delta T_{fm} = T_f - \Delta T_{fs}$ into the Equation (2), we obtain

$$\Psi_f = \frac{L}{g} \ln \left(\frac{T_0 + \Delta T_{fm}}{T_0} \right) = \frac{L}{g} \ln \left(\frac{T_f - \Delta T_{fs}}{T_0} \right) \tag{9}$$

Then, a new expression describing the SFCC is obtained for saline soil as follows:

$$\theta_l = \theta_r + (\theta_s - \theta_r) \left(1 + \left(\alpha \frac{L_f}{g} \ln \left(\frac{T_f - \Delta T_{fs}}{T_0} \right) \right)^n \right)^{-m}, \psi_f < \psi_u \tag{10}$$

Assuming the soil salt is purely NaCl, which forms NaCl·H₂O when the temperature is below 0.1 °C [43,61], the relationship between the freezing point depression induced by solute concentrate (ΔT_{fs}) and the salt concentration (c) is provided by Wang et al. [43]:

$$\Delta T_{fs} / T^* = \varphi(c) = \sum_{i=0}^5 \left(Z_i (100c_w)^i \right) \tag{11}$$

where $z_0 = 0$, $z_1 = -0.5697$, $z_2 = -1 \times 10^{-3}$, $z_3 = -1 \times 10^{-4}$, $z_4 = 2 \times 10^{-6}$, and $z_5 = -8 \times 10^{-8}$. T^* (=1K) is aimed to normalize the value of temperature and c_w (g·L⁻¹) is the salt concentration, i.e., mass of salt per unit volume of water.

Notably, in this study, we assume that the change in solute concentration is only associated with the change in liquid water content change but neglects the transport and

redistribution of solute following [1,41]. The structure of soil is assumed as the capillary model, which is the most general physical model when we describe the SFCC in soil [62].

2.2. Lab and Field Experiments

2.2.1. Laboratory Experiments

To test the performance of the proposed GCE-salt model in capturing the SFCC, lab experiments measuring the SFCC of soils of different salinity were conducted. The soil sample was collected from one farmland near the Shahaoqu Experimental Station, in the Hetao Irrigation District, China (about 40.908° N, 107.158° E) (Figure 1), which is mainly planted with wheat. Soil was dug from one agricultural field at the depth of 0 to 20 cm, where salinization was the most serious. This soil sample was classified as a sandy loam according to USDA classification methods. It is the most common soil texture in Hetao Irrigation District. This area is a typical seasonal frozen area [63] and a typical saline arid and semi-arid area due to long-term irrigation [57]. The soil sample was flushed by deionized water to salinity below 0.05% to eliminate the background salinity. After sieving by 2 mm sieve and air-drying, the basic characteristics of the soil sample are shown in Table 1. Four soil samples were mainly used to demonstrate the influence of the salt concentration on the SFCC. The sandy loam (32.6% sand, 61.3% silt, and 6.1% clay) was treated to a target VWC of $0.35 \text{ cm}^3 \cdot \text{cm}^{-3}$ and four different soil salinities (salinity (SS) = 0%, 0.2%, 0.4%, and 0.6%, equivalent to NaCl concentration (c_w) of 0, 0.75, 1.50, and 2.25 $\text{g} \cdot \text{L}^{-1}$), which are categorized as non-saline, slightly saline, moderately saline, and highly saline soil, respectively, according to [64].

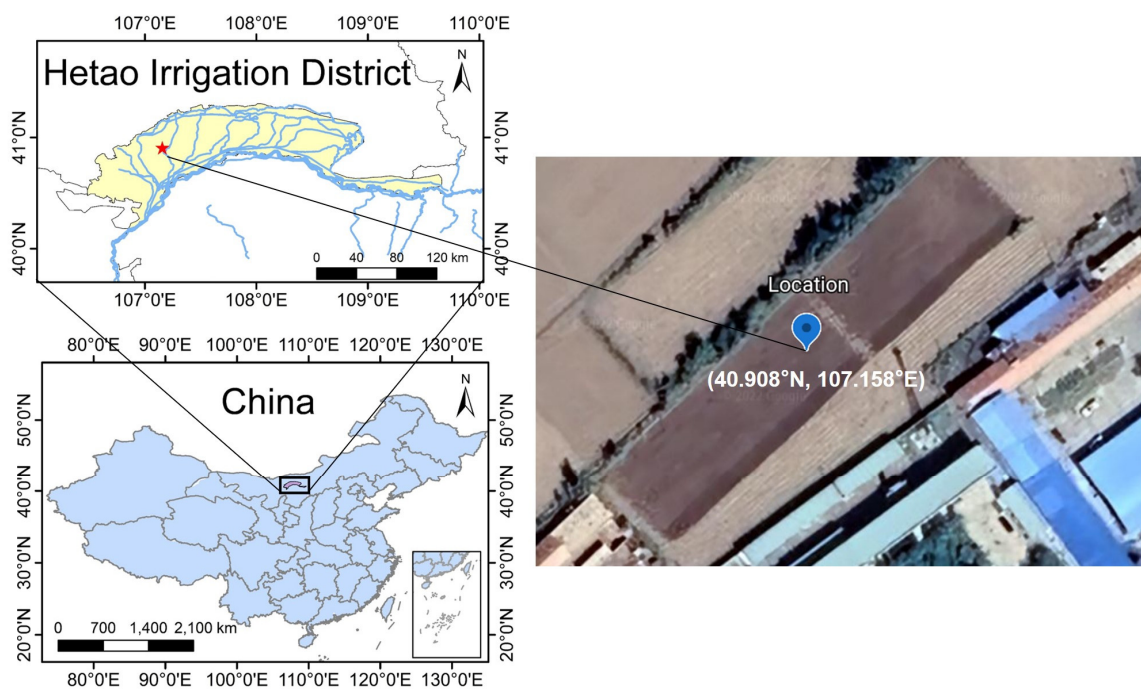


Figure 1. Location of the Hetao Irrigation District and the location of the sampling point of the laboratory experiments.

Table 1. The basic characteristics of soil in the study area.

Soil Types	Particle Distribution/%			Specific Surface Area $\text{m}^2 \cdot \text{g}^{-1}$	Bulk Density $\text{g} \cdot \text{cm}^{-3}$
	0.01–2.00 μm	2.00–50.00 μm	50.00–2000.00 μm		
Sandy loam ^a	6.078	61.258	32.644	0.743	1.5

Note: ^a a soil texture determined from the USDA Soil Texture Triangle.

The wet soil was then packed into columns of 10 cm diameter and 13 cm length by 5 cm increments to reach a bulk density of $1.5 \text{ g}\cdot\text{cm}^{-3}$. The experimental soil volume fully encompassed the maximum measurement volume of the 5TE sensor [65].

One pre-calibrated 5TE Meter (Meter Group Inc., Pullman, WA, USA) was inserted vertically into each packed soil (Figure 2b). Each of the used 5TE Meter were calibrated for the effect of initial salt concentration on the dielectric constant based on the 5TE manual [65]. The packed soil samples were placed in a temperature control chamber (Figure 2a) (XT5438-TC250-R35, Xutemp, Hangzhou, China) to experience a freezing–thawing process (Figure 2c).

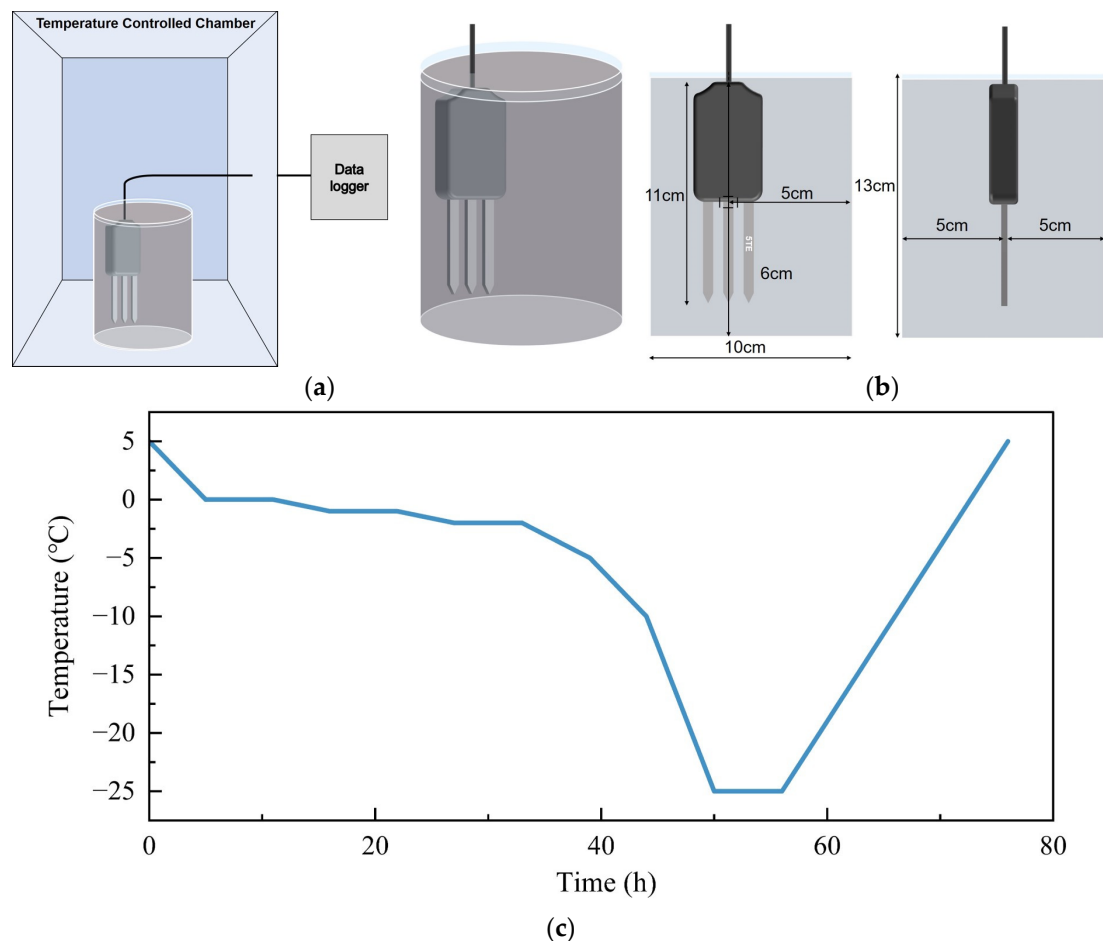


Figure 2. Lab experiment setup: (a) a soil column in the temperature controlled chamber, (b) the position of a 5TE sensor in a soil column, and (c) the freezing–thawing condition.

2.2.2. Field Experiment

To test the performance of the GCE-Salt Model in capturing the SFCC of in situ soil of different salinities, a field experiment was conducted during the 2017–2018 freezing–thawing period at the Shahaoqu Station in the Hetao Irrigation District, China (Figure 1). Two neighboring test fields were selected: one extremely saline abandoned land (SAL) and one slightly saline cropland (CL1). Wang et al. [10] tested that the soil condition was homogeneous in the same farmland, so we picked a point in the same soil to represent the nature of the site. The soil temperature and soil moisture of the soil profiles were monitored at 20, 40, 60, 100, and 140 cm depth hourly by Hydra Probe sensors (Stevens Water Monitoring Systems, Inc., Portland, Oregon, USA) [66]. The inherent fundamental assumption of the GCE-based SFCC models is that the ice formation reduced the soil water potential and the liquid water content. Thus, the field data used to test GCE-based models must meet the requirement that the total soil water content does not change significantly

during the testing period. If the total soil water content changes, then, the soil water potential and the liquid water content would be interfered by other factors, not solely ice formation any more, and the GCE-based models may fail.

At our study site, the groundwater table was very shallow, from about 0.5 m to 2.5 m during the freezing period, and only the 0–20 cm has a nearly constant total soil water content during the freezing period [66]. Thus, only the data of the 0–20 cm topsoil were used for the model performance testing to meet the fundamental assumption of GCE-based models (Figure 3).

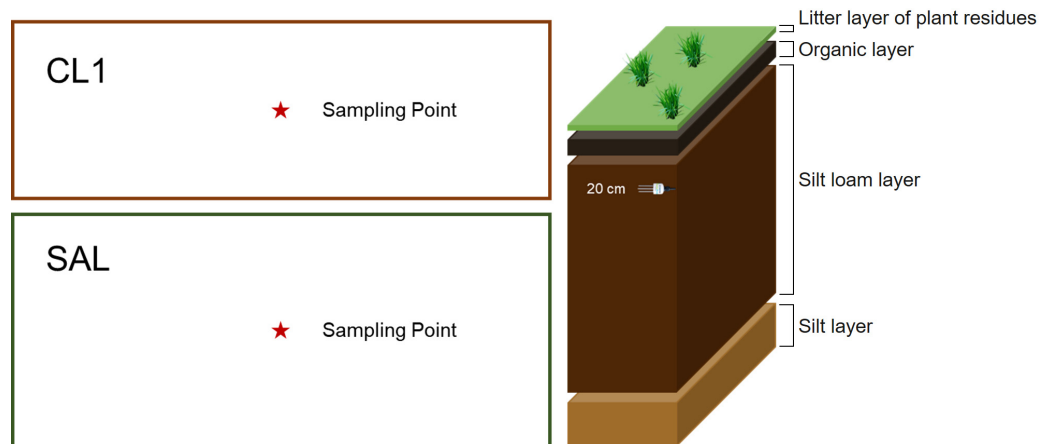


Figure 3. Sampling point of the field experiment and test equipment. The stars on the left figure illustrate the location of sampling points in the fields, and the right figure illustrates the vertical structure of soil layers in the field.

The soil particle distribution was measured by a Mastersizer 2000 (Malvern Instruments Ltd., Malvern, UK) to determine soil texture (Table 2). The soil bulk density was determined by oven drying at 105 °C. The dominant salt at the study site is NaCl [66]. The soil salinity was determined by measuring $EC_{1:5}$ ($mS \cdot cm^{-1}$) and converting it to soil salinity (SS, %) by $SS = 3.480 EC_{1:5} - 0.236$ ($R^2 = 0.993$) following Liu et al. [67]. The saturated water content (θ_s) was obtained as the highest in situ VWC after flood irrigation during the cropping season [67]; whereas, the residual water content (θ_r) was obtained as the lowest in situ liquid water content during the stable frozen period [31,66]. The inverse of the air-entry value (α) and the pore-size distribution index (n) were calibrated by fitting the GCE model to the measured SFCC.

Table 2. The soil properties of the experimental fields.

SITE	Sand (%) ^a	Silt (%) ^a	Clay (%) ^a	Texture ^d	ρ_b ($g \cdot cm^{-3}$) ^a	θ_r ($cm^3 \cdot cm^{-3}$) ^b	θ_s ($cm^3 \cdot cm^{-3}$) ^b	α (m^{-1}) ^c	n ^c
SAL	35.39	58.03	6.57	silt loam	1.51	0.046	0.479	0.080	1.171
CL1	25.66	61.76	12.58	silt loam	1.53	0.101	0.450	0.047	2.354

Note: ^a lab measured. ^b field monitored. ^c calibrated by fitting GCE to measured SFCC. ^d according to USDA.

3. Results and Discussion

In the results and discussion, we tested the performance of the proposed GCE-Salt Model in both non-saline soil and saline soil and compared it with the models introduced in the introduction. We compared the GCE-Salt Model with the Combined Model in non-saline, which is the well-performing model that has been validated in non-saline soils. We reached the GCE-Salt Model with the Combined Model and GCE-Tan Model, both of which have been validated in the field and indoor experiments compared to other models proposed in recent years.

3.1. Lab Non-Saline Soil

For non-saline soil (Figure 4), both the Combined Model and the GCE-Salt Model are basically just the GCE Model (Equation (4)). Thus, the three models overlap and behave equally well (the root mean squared error (RMSE) = 0.037 cm³·cm⁻³ and the Nash–Sutcliffe efficiency coefficient (NSE) = 0.866). All three models simulate the lower part of the unfrozen water content (<0.1 cm³·cm⁻³) well and all of them slightly overestimate the unfrozen water content at the rapid drop part (from 0.34 to 0.07 cm³·cm⁻³). The outliers were due to supercooling, i.e., at the beginning of a relatively fast freezing, the soil temperature rapidly dropped to the temperature of spontaneous nucleation but the liquid water could not release latent heat and turn into ice fast enough [1,42].

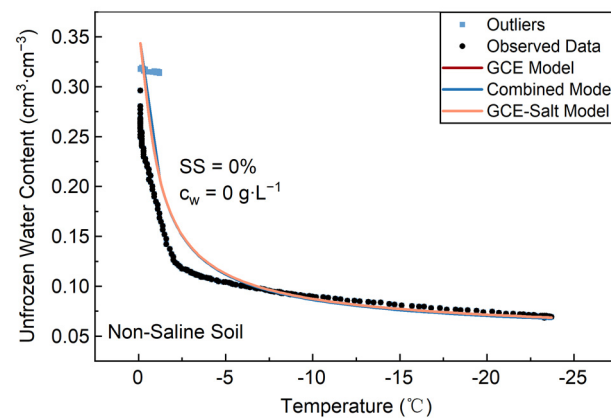


Figure 4. The observed lab non-saline soil SFCC and the simulated SFCC by the GCE Model, the Combined Model, and the GCE-Salt Model.

3.2. Saline Soil

To further test the performance of the GCE-Salt Model in different concentrations, we compared the performance of the GCE-Tan Model proposed by Tan et al. [46], the Combined Model, proposed by Amankwah et al. [1], and the GCE-Salt Model both in small sample lab and field experiments.

3.2.1. Lab Slightly to Highly Saline Soils

Our GCE-Salt Model performed similarly well as the Combined Model and the GCE-Tan Model for the lab slightly to highly saline soil (Figure 5, NSE ≥ 0.80 and RMSE < 0.030 cm³·cm⁻³ for the three models). Particularly, compared to the GCE-Tan Model (RMSE = 0.029 cm³·cm⁻³, NSE = 0.90), both the Combined Model (RMSE = 0.023 cm³·cm⁻³, NSE = 0.93) and the GCE-Salt Model (RMSE = 0.024 cm³·cm⁻³, NSE = 0.94) have remarkably high accuracy for the highly saline soil (Figure 5c). Whereas, they all overestimated the unfrozen water content at the rapid dropping stage for the slightly and moderately saline soils (Figure 5a,b). These indicated that the 0.4% soil salinity might not be high enough to illustrate the ability of the models in dealing with solute induced freezing point depression. As a common phenomenon in lab freezing experiments [59,68], supercooling occurred in all these lab saline soils, too. The fitted soil parameters are the same as the value of the non-saline soil (Table 3) and the transport and redistribution of salt in the soil were considered negligible [1].

Table 3. The shared fitted parameters of the GCE model, the Combined Model, and the GCE-Salt model for the lab non-saline soil.

Parameter	α (m ⁻¹)	n	m	θ_s (cm ³ ·cm ⁻³)	θ_r (cm ³ ·cm ⁻³)
Value	0.014	1.69	0.41	0.40	0.046

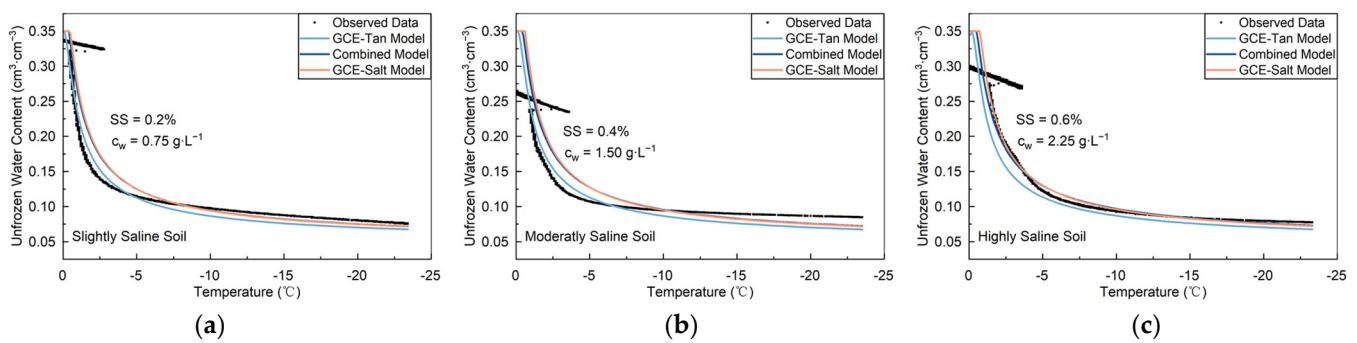


Figure 5. The observed lab of slightly to highly saline soil SFCC and the simulated SFCC by the GCE-Tan Model, Combined Model, and the GCE-Salt Model at three different salinity levels ((a) slightly (SS = 0.2%, $c_w = 0.75 \text{ g}\cdot\text{L}^{-1}$), (b) moderately (SS = 0.4%, $c_w = 1.50 \text{ g}\cdot\text{L}^{-1}$), and (c) highly (SS = 0.6%, $c_w = 2.25 \text{ g}\cdot\text{L}^{-1}$) saline soil) at a target moisture content of $0.35 \text{ cm}^3\cdot\text{cm}^{-3}$.

3.2.2. Field Extremely and Slightly Saline Soils

Then, the ability of our newly proposed GCE-Salt model to capture the SFCC, especially the freezing point, at different salinity levels was tested with a slightly saline cropland (CL1) and an extremely saline abandoned land (SAL) (Table 4), against the GCE-Tan Model and the Combined Model (Figure 6a,b). The GCE-Salt Model (RMSE = $0.013 \text{ cm}^3\cdot\text{cm}^{-3}$, NSE = 0.99) performed similarly well as the Combined Model (RMSE = $0.017 \text{ cm}^3\cdot\text{cm}^{-3}$, NSE = 0.98) for the slightly saline soil (Figure 6a) and performed slightly better than the GCE-Tan Model (RMSE = $0.098 \text{ cm}^3\cdot\text{cm}^{-3}$, NSE = 0.94). Both the Combined Model and the GCE-Salt Model captured the unfrozen water content at the rapid dropping stage well and at the residue part ($0.10 \text{ cm}^3\cdot\text{cm}^{-3}$). Whereas, the GCE-Salt Model (RMSE = $0.013 \text{ cm}^3\cdot\text{cm}^{-3}$, NSE = 0.92) surpassed the GCE-Tan Model (RMSE = $0.029 \text{ cm}^3\cdot\text{cm}^{-3}$, NSE = 0.62) and the Combined Model (RMSE = $0.017 \text{ cm}^3\cdot\text{cm}^{-3}$, NSE = 0.86) on the extremely saline soil (Figure 6b). Comparing the better-performed Combined Model and the GCE-Salt Model, the Combined Model better captured the elevated residue unfrozen water content ($0.25 \text{ cm}^3\cdot\text{cm}^{-3}$); whereas, the GCE-Salt Model overestimated that by $0.26 \text{ cm}^3\cdot\text{cm}^{-3}$. However, the GCE-Salt Model accurately captured the huge freezing point depression of -1.70 K ; whereas, the Combined Model underestimated this freezing point depression by 0.7 K .

Table 4. Parameters of the fitting by the selected models for field soil.

Site	SS (%)	c_w ($\text{g}\cdot\text{L}^{-1}$)	Model	RMSE ($\text{cm}^3\cdot\text{cm}^{-3}$)	NSE
CL1	0.05	0.16	GCE-Tan Model	0.098	0.94
			Combined Model	0.017	0.98
			GCE-Salt Model	0.013	0.99
SAL	1.18	3.72	GCE-Tan Model	0.029	0.62
			Combined Model	0.017	0.86
			GCE-Salt Model	0.013	0.92

The T_m (-0.35 K) in the GCE-Tan Model is smaller than the T_m in the Combined Model and the GCE-Salt Model, suggesting that this model would underestimate the effect of salinity on the freezing point. However, the T_m (-0.49 K) in the Combined Model and the ΔT_{fs} (-0.44 K) in the GCE-Salt Model are similar, indicating that the estimation of the freezing point depression induced by solute potential is not the fundamental difference between the two models. In other words, keeping the Ψ_f as the soil matric potential and excluding the effect of solute potential in the numerator proved to be a better approach to capturing the freezing point than regarding the Ψ_f as the summation of soil matric potential and solute potential and considering the effect of soil matric potential and the effect of solute potential in the numerator and denominator, respectively.

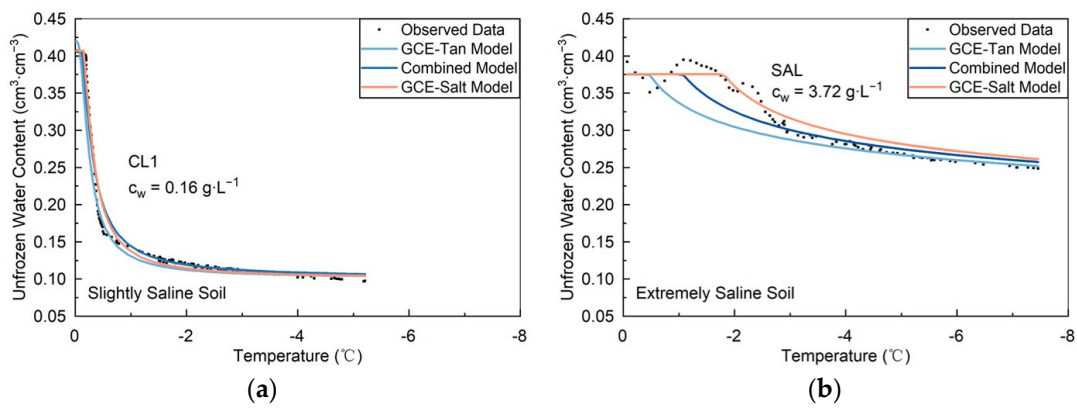


Figure 6. The observed field of extremely ((a) from the CL1) and slightly ((b) from the SAL) saline soil SFCC and the simulated SFCC by the GCE-Tan Model, Combined Model, and the GCE-Salt Model.

To reveal the fundamental difference between the Combined Model and the GCE-Salt Model at capturing the freezing point, the SFCC of the SAL soil (soil properties are listed in Table 3) was simulated at different salinity levels: 0, 3.0 g·L⁻¹, 3.72 g·L⁻¹ (same as the in situ salinity), and 4.5 g·L⁻¹ (Figure 7). The estimated freezing points by the two models are significantly different at $c_w = 3.0 \text{ g}\cdot\text{L}^{-1}$: the difference has reached 0.63 K. This difference becomes more and more significant with the increase in salinity, reaching 1.85 K when $c_w = 4.5 \text{ g}\cdot\text{L}^{-1}$. The two models eventually converge at the same residue unfrozen water content.

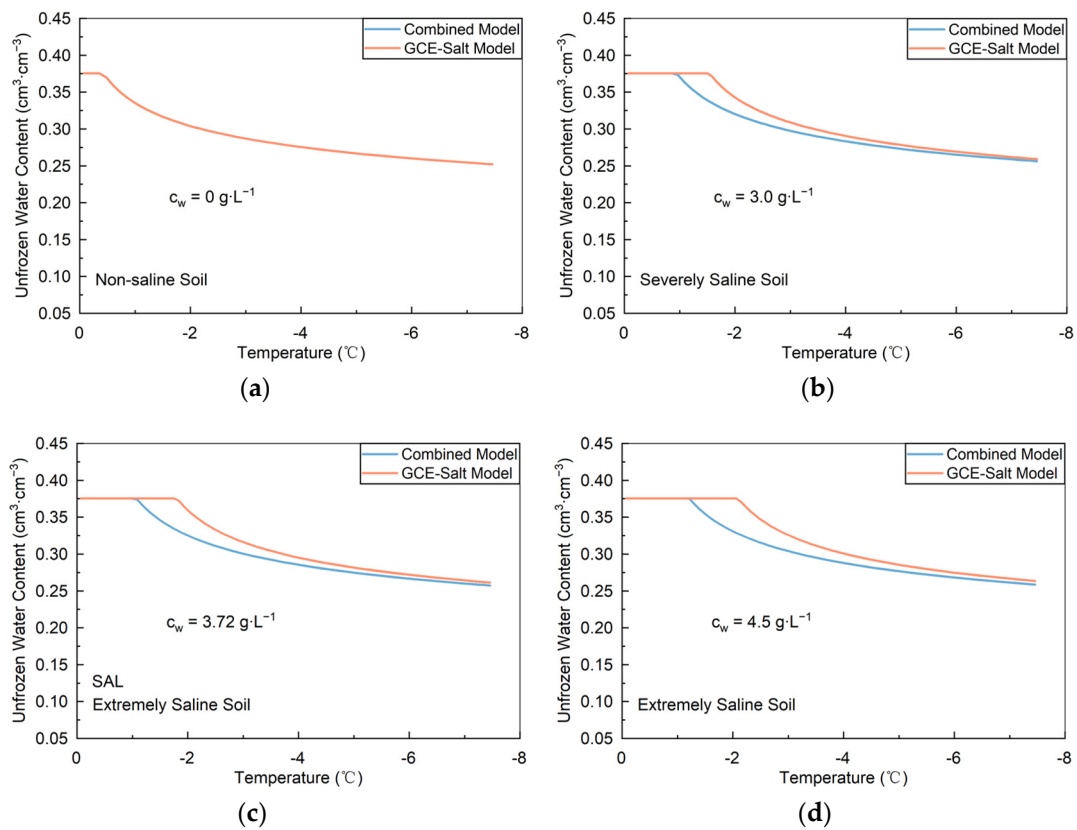


Figure 7. Comparing the Combined Model and GCE-Salt Model under different soil salinity levels. ((a) non-saline ($c_w = 0 \text{ g}\cdot\text{L}^{-1}$), (b) severely ($c_w = 3.0 \text{ g}\cdot\text{L}^{-1}$), (c) extremely ($c_w = 3.72 \text{ g}\cdot\text{L}^{-1}$) and (d) extremely ($c_w = 4.5 \text{ g}\cdot\text{L}^{-1}$) saline soil) at the SAL soil properties.

The ability of our newly proposed GCE-Salt Model to capture the SFCC was first tested without salt against the Combined Model. Then, the performance of the GCE-Salt Model, especially, capturing the freezing point at different salinity levels against the GCE-Tan Model and the Combined Model was tested with sandy loam at slightly, moderately, and highly saline levels in the lab temperature-controlled chamber and in situ silt loam at slightly and extremely saline levels. Soils of different textures and at different salinity levels, particularly highly, severely, and extremely saline levels, could be used to test the ability of the GCE-Salt Model to capture the SFCC against the GCE-Tan Model and the Combined Model, to more comprehensively reveal which expression could better capture the freezing point of SFCC in saline soil.

4. Conclusions

In this study, we propose a novel model based on the Generalized Clapeyron Equation (GCE), the GCE-Salt Model to simulate the soil freezing characteristic curve (SFCC) in frozen saline soil accurately. By keeping the Ψ_f in the GCE as the matric potential and by incorporating solute potential, our model precisely captures the equilibrium freezing temperature (Ψ_f) and has shown excellent performance in both lab and field experiments, especially in extremely saline soil. Our GCE-Salt Model helps better understand the freezing and thawing of saline soil, which would promote a better understanding of the effect of the seasonal freezing–thawing cycle on the thermal–hydrological processes and the structure of saline soil.

The performance of our GCE-Salt Model was validated by both lab and field experimental data and compared with previous models: (1) our GCE-Salt Model could capture the SFCC of non-saline soil equally as well as the Combined Model. (2) Our GCE-Salt Model performed better than the GCE-Tan Model and performed similarly well as the Combined Model for the slightly to highly saline soil. (3) Our GCE-Salt Model beat the Combined Model and the GCE-Tan Model in capturing the SFCC of extremely saline soil, mainly because it can more accurately capture the freezing point.

For future studies, it is highly recommended to test the ability of the GCE-Salt Model to capture the SFCC with soils of different textures and at different salinity levels, particularly highly, severely, and extremely saline levels, to more comprehensively reveal which expression could better capture the SFCC in saline soil.

Author Contributions: Conceptualization, L.W. and Z.H.; methodology, L.W.; software, L.W.; validation, L.W., X.W. and Z.H.; formal analysis, L.W.; investigation, L.W.; resources, L.W., J.H. and X.W.; data curation, L.W., J.H. and X.W.; writing—original draft preparation, L.W.; writing—review and editing, L.W., X.W. and C.W.; visualization, L.W.; supervision, C.W., C.Z. and Z.H.; project administration, C.W., C.Z. and Z.H.; funding acquisition, Z.H.; All authors have read and agreed to the published version of the manuscript.

Funding: This work was supported by the National Natural Science Foundation of China [grant numbers: 52130902] and the National Key Research and Development Program of China [grant number: 2021YFD1900603].

Data Availability Statement: The lab and field experiment data used for the validation of the model in the study are available via reasonable request from the corresponding author, Zailin Huo, via email: huozl@cau.edu.cn.

Acknowledgments: The authors would like to thank Shahaoqu Experimental Station, Inner Mongolia Hetao Irrigation District Jiefangzha Department, China, for their assistance with the experimental setup and field work.

Conflicts of Interest: The authors declare no conflicts of interest.

References

- Amankwah, S.K.; Ireson, A.M.; Maulé, C.; Brannen, R.; Mathias, S.A. A Model for the Soil Freezing Characteristic Curve That Represents the Dominant Role of Salt Exclusion. *Water Resour. Res.* **2021**, *57*, e2021WR030070. [\[CrossRef\]](#)
- He, H.; Dyck, M.; Zhao, Y.; Si, B.; Jin, H.; Zhang, T.; Lv, J.; Wang, J. Evaluation of five composite dielectric mixing models for understanding relationships between effective permittivity and unfrozen water content. *Cold Reg. Sci. Technol.* **2016**, *130*, 33–42. [\[CrossRef\]](#)
- Gao, B.; Yang, D.; Qin, Y.; Wang, Y.; Li, H.; Zhang, Y.; Zhang, T. Change in frozen soils and its effect on regional hydrology, upper Heihe basin, northeastern Qinghai–Tibetan Plateau. *Cryosphere* **2018**, *12*, 657–673. [\[CrossRef\]](#)
- Kong, F.; Nie, L.; Xu, Y.; Rui, X.; He, Y.; Zhang, T.; Wang, Y.; Du, C.; Bao, C. Effects of freeze-thaw cycles on the erodibility and microstructure of soda-saline loessal soil in Northeastern China. *Catena* **2022**, *209*, 105812. [\[CrossRef\]](#)
- Gharedaghlou, B.; Berg, S.J.; Sudicky, E.A. Water freezing characteristics in granular soils: Insights from pore-scale simulations. *Adv. Water Resour.* **2020**, *143*, 103681. [\[CrossRef\]](#)
- Krzeminska, D.; Bloem, E.; Starkloff, T.; Stolte, J. Combining FDR and ERT for monitoring soil moisture and temperature patterns in undulating terrain in south-eastern Norway. *Catena* **2022**, *212*, 106100. [\[CrossRef\]](#)
- Ding, B.; Zhang, Y.; Yu, X.; Jia, G.; Wang, Y.; Zheng, P.; Li, Z. Comparative study of seasonal freeze–thaw on soil water transport in farmland and its shelterbelt. *Catena* **2023**, *225*, 106982. [\[CrossRef\]](#)
- Xu, J.; Ren, J.; Wang, Z.; Wang, S.; Yuan, J. Strength behaviors and meso-structural characters of loess after freeze-thaw. *Cold Reg. Sci. Technol.* **2018**, *148*, 104–120. [\[CrossRef\]](#)
- Hou, R.; Li, T.; Fu, Q.; Liu, D.; Li, M.; Zhou, Z.; Li, L.; Yan, J. Characteristics of water–heat variation and the transfer relationship in sandy loam under different conditions. *Geoderma* **2019**, *340*, 259–268. [\[CrossRef\]](#)
- Wang, X.; Wang, C.; Wang, X.; Huo, Z. Response of soil compaction to the seasonal freezing–thawing process and the key controlling factors. *Catena* **2020**, *184*, 104247. [\[CrossRef\]](#)
- Ye, W.; Li, C. The consequences of changes in the structure of loess as a result of cyclic freezing and thawing. *Bull. Eng. Geol. Environ.* **2018**, *78*, 2125–2138. [\[CrossRef\]](#)
- Ren, J.; Vanapalli, S.K.; Han, Z. Soil freezing process and different expressions for the soil-freezing characteristic curve. *Sci. Cold Arid Reg.* **2017**, *9*, 221–228. [\[CrossRef\]](#)
- Xiao, Z.; Lai, Y.; Zhang, M. Study on the freezing temperature of saline soil. *Acta Geotech.* **2017**, *13*, 195–205. [\[CrossRef\]](#)
- Wu, M.; Tan, X.; Huang, J.; Wu, J.; Jansson, P.-E. Solute and water effects on soil freezing characteristics based on laboratory experiments. *Cold Reg. Sci. Technol.* **2015**, *115*, 22–29. [\[CrossRef\]](#)
- Wu, Y.; Wang, Y.; Hu, L. A theoretical model of the soil freezing characteristic curve for saline soil. *J. Hydrol.* **2023**, *622*, 129639. [\[CrossRef\]](#)
- Chen, J.; Mei, S.; Irizarry, J.T.; Rempel, A.W. A Monte Carlo Approach to Approximating the Effects of Pore Geometry on the Phase Behavior of Soil Freezing. *J. Adv. Model. Earth Syst.* **2020**, *12*, e2020MS002117. [\[CrossRef\]](#)
- Bi, J.; Wang, G.; Wu, Z.; Wen, H.; Zhang, Y.; Lin, G.; Sun, T. Investigation on unfrozen water content models of freezing soils. *Front. Earth. Sci.* **2023**, *10*, 1039330. [\[CrossRef\]](#)
- Chai, M.; Zhang, J.; Zhang, H.; Mu, Y.; Sun, G.; Yin, Z. A method for calculating unfrozen water content of silty clay with consideration of freezing point. *Appl. Clay Sci.* **2018**, *161*, 474–481. [\[CrossRef\]](#)
- Li, Z.; Chen, J.; Sugimoto, M. Pulsed NMR Measurements of Unfrozen Water Content in Partially Frozen Soil. *J. Cold Reg. Eng.* **2020**, *34*, 04020013. [\[CrossRef\]](#)
- Teng, J.; Zhong, Y.; Zhang, S.; Sheng, D. A mathematic model for the soil freezing characteristic curve: The roles of adsorption and capillarity. *Cold Reg. Sci. Technol.* **2021**, *181*, 103178. [\[CrossRef\]](#)
- Bittelli, M.; Flury, M.; Campbell, G.S. A thermodielectric analyzer to measure the freezing and moisture characteristic of porous media. *Water Resour. Res.* **2003**, *39*, 1041. [\[CrossRef\]](#)
- Nishimura, S.; Gens, A.; Olivella, S.; Jardine, R.J. THM-coupled finite element analysis of frozen soil: Formulation and application. *Geotechnique* **2009**, *59*, 159–171. [\[CrossRef\]](#)
- Zhou, J. *Experimental Study on Characteristics of Unfrozen Water in Clay Mineral and Its Effect on Sand Thawing Characteristics*; China University of Mining and Technology: Xuzhou, China, 2020.
- Wen, Z.; Ma, W.; Feng, W.; Deng, Y.; Wang, D.; Fan, Z.; Zhou, C. Experimental study on unfrozen water content and soil matric potential of Qinghai-Tibetan silty clay. *Environ. Earth Sci.* **2011**, *66*, 1467–1476. [\[CrossRef\]](#)
- Dall’Amico, M.; Endrizzi, S.; Gruber, S.; Rigon, R. A robust and energy-conserving model of freezing variably-saturated soil. *Cryosphere* **2011**, *5*, 469–484. [\[CrossRef\]](#)
- Anderson, D.M.; Tice, A.R. Predicting Unfrozen Water Contents in Frozen Soils from Surface Area Measurements. *Highw. Res. Rec.* **1972**, *393*, 12–18.
- Michalowski, R.L.; Zhu, M. Frost heave modelling using porosity rate function. *Int. J. Numer. Anal. Methods Geomech.* **2006**, *30*, 703–722. [\[CrossRef\]](#)
- Michalowski, R.L. A constitutive model of saturated soils for frost heave simulations. *Cold Reg. Sci. Technol.* **1993**, *22*, 47–63. [\[CrossRef\]](#)
- Osterkamp, T.E.; Romanovsky, V.E. Freezing of the Active Layer on the Coastal Plain of the Alaskan Arctic. *Permafr. Periglac. Process.* **1997**, *8*, 23–44. [\[CrossRef\]](#)

30. McKenzie, J.M.; Voss, C.I.; Siegel, D.I. Groundwater flow with energy transport and water–ice phase change: Numerical simulations, benchmarks, and application to freezing in peat bogs. *Adv. Water Resour.* **2007**, *30*, 966–983. [[CrossRef](#)]
31. Kozłowski, T. A semi-empirical model for phase composition of water in clay–water systems. *Cold Reg. Sci. Technol.* **2007**, *49*, 226–236. [[CrossRef](#)]
32. Zhang, Y.; Carey, S.K.; Quinton, W.L. Evaluation of the algorithms and parameterizations for ground thawing and freezing simulation in permafrost regions. *J. Geophys. Res.* **2008**, *113*, 116. [[CrossRef](#)]
33. Nicolsky, D.J.; Romanovsky, V.E.; Panda, S.K.; Marchenko, S.S.; Muskett, R.R. Applicability of the ecosystem type approach to model permafrost dynamics across the Alaska North Slope. *J. Geophys. Res. Earth Surf.* **2017**, *122*, 50–75. [[CrossRef](#)]
34. Weng, L.; Wu, Z.; Liu, Q.; Chu, Z.; Zhang, S. Evolutions of the unfrozen water content of saturated sandstones during freezing process and the freeze-induced damage characteristics. *Int. J. Rock Mech. Min. Sci.* **2021**, *142*, 104757. [[CrossRef](#)]
35. Westermann, S.; Boike, J.; Langer, M.; Schuler, T.V.; Etzelmüller, B. Modeling the impact of wintertime rain events on the thermal regime of permafrost. *Cryosphere* **2011**, *5*, 945–959. [[CrossRef](#)]
36. Li, B.; Huang, L.; Lv, X.; Ren, Y. Variation features of unfrozen water content of water-saturated coal under low freezing temperature. *Sci. Rep.* **2021**, *11*, 15398. [[CrossRef](#)]
37. Qin, Y.; Li, G.; Qu, G. A formula for the unfrozen water content and temperature of frozen soils. In *Cold Regions Engineering 2009: Cold Regions Impacts on Research, Design, and Construction*; 2009; pp. 155–161. Available online: [https://ascelibrary.org/doi/10.1061/41072\(359\)18](https://ascelibrary.org/doi/10.1061/41072(359)18) (accessed on 15 January 2023).
38. Kong, L.; Wang, Y.; Sun, W.; Qi, J. Influence of plasticity on unfrozen water content of frozen soils as determined by nuclear magnetic resonance. *Cold Reg. Sci. Technol.* **2020**, *172*, 102993. [[CrossRef](#)]
39. Kurylyk, B.L.; Watanabe, K. The mathematical representation of freezing and thawing processes in variably-saturated, non-deformable soils. *Adv. Water Resour.* **2013**, *60*, 160–177. [[CrossRef](#)]
40. Ma, T.; Wei, C.; Xia, X.; Zhou, J.; Chen, P. Soil Freezing and Soil Water Retention Characteristics: Connection and Solute Effects. *J. Perform. Constr. Fac.* **2017**, *31*, D4015001. [[CrossRef](#)]
41. Zhou, J.; Wei, C.; Lai, Y.; Wei, H.; Tian, H. Application of the Generalized Clapeyron Equation to Freezing Point Depression and Unfrozen Water Content. *Water Resour. Res.* **2018**, *54*, 9412–9431. [[CrossRef](#)]
42. Zhou, J.; Meng, X.; Wei, C.; Pei, W. Unified Soil Freezing Characteristic for Variably-Saturated Saline Soils. *Water Resour. Res.* **2020**, *56*, e2019WR026648. [[CrossRef](#)]
43. Wang, L.; Liu, J.; Yu, X.; Wang, T.; Feng, R. A Simplified Model for the Phase Composition Curve of Saline Soils Considering the Second Phase Transition. *Water Resour. Res.* **2021**, *57*, e2020WR028556. [[CrossRef](#)]
44. Wan, X.; Yang, Z. Pore water freezing characteristic in saline soils based on pore size distribution. *Cold Reg. Sci. Technol.* **2020**, *173*, 103030. [[CrossRef](#)]
45. Wang, L.; Wang, P.; Liu, J.; Liu, J.; Chen, W.; Zhang, Q.; Wang, T. Crystallization deformation and phase transitions of coarse-grained sulfate saline soils upon cooling. *Cold Reg. Sci. Technol.* **2023**, *209*, D4015001. [[CrossRef](#)]
46. Tan, X.; Wu, M.; Huang, J.; Wu, J.; Chen, J. Similarity of soil freezing characteristic and soil water characteristic: Application in saline frozen soil hydraulic properties prediction. *Cold Reg. Sci. Technol.* **2020**, *173*, 102876. [[CrossRef](#)]
47. Xu, X.; Oliphant, J.L.; Tice, A.R. Prediction of unfrozen water content in frozen soil by a two-point or one-point method. In *Proceedings of the 4th International Symposium on Ground Freezing, Sapporo, Japan, 5–7 August 1985; Volume 2*, pp. 83–87.
48. Banin, A.; Anderson, D.M. Effects of Salt Concentration Changes During Freezing on the Unfrozen Water Content of Porous Materials. *Water Resour. Res.* **1974**, *10*, 124–128. [[CrossRef](#)]
49. Bi, J.; Wu, Z.; Lu, Y.; Wen, H.; Zhang, Y.; Shen, Y.; Wei, T.; Wang, G. Study on soil freezing characteristic curve during a freezing–thawing process. *Front. Earth. Sci.* **2023**, *10*, 1007342. [[CrossRef](#)]
50. Jin, X.; Yang, W.; Gao, X.; Zhao, J.Q.; Li, Z.; Jiang, J. Modeling the Unfrozen Water Content of Frozen Soil Based on the Absorption Effects of Clay Surfaces. *Water Resour. Res.* **2020**, *56*, e2020WR027482. [[CrossRef](#)]
51. Wang, C.; Li, S.; Lai, Y.; Chen, Q.; He, X.; Zhang, H.; Liu, X. Predicting the Soil Freezing Characteristic From the Particle Size Distribution Based on Micro-Pore Space Geometry. *Water Resour. Res.* **2022**, *58*, e2021WR030782. [[CrossRef](#)]
52. Dall’Amico, M. Coupled Water and Heat Transfer in Permafrost Modeling. Doctoral Thesis, University of Trento, Trento, Italy, 2010.
53. Sheshukov, A.Y.; Nieber, J.L. One-dimensional freezing of nonheaving unsaturated soils: Model formulation and similarity solution. *Water Resour. Res.* **2011**, *47*, W11519. [[CrossRef](#)]
54. Liu, Z.; Yu, X. Physically Based Equation for Phase Composition Curve of Frozen Soils. *Transp. Res. Rec. J. Transp. Res. Board* **2013**, *2349*, 93–99. [[CrossRef](#)]
55. Mu, Q.Y.; Ng, C.W.W.; Zhou, C.; Zhou, G.G.D.; Liao, H.J. A new model for capturing void ratio-dependent unfrozen water characteristics curves. *Comput. Geotech.* **2018**, *101*, 95–99. [[CrossRef](#)]
56. Wen, H.; Bi, J.; Guo, D. Evaluation of the calculated unfrozen water contents determined by different measured subzero temperature ranges. *Cold Reg. Sci. Technol.* **2020**, *170*, 102927. [[CrossRef](#)]
57. Wang, C.; Luo, Y.; Huo, Z.; Liu, Z.; Liu, G.; Wang, S.; Lin, Y.; Wu, P. Salt Accumulation during Cropping Season in an Arid Irrigation Area with Shallow Water Table Depth: A 10-Year Regional Monitoring. *Water* **2022**, *14*, 1664. [[CrossRef](#)]
58. Fuchs, M.; Campbell, G.S.; Papendick, R.I. An Analysis of Sensible and Latent Heat Flow in a Partially Frozen Unsaturated Soil. *Soil Sci. Soc. Am. J.* **1978**, *42*, 379–385. [[CrossRef](#)]

59. Wan, X.; Liu, E.; Qiu, E. Study on ice nucleation temperature and water freezing in saline soils. *Permaf. Periglac. Process.* **2020**, *32*, 119–138. [[CrossRef](#)]
60. Van Genuchten, M.T. A closed-form equation for predicting the hydraulic conductivity of unsaturated soils. *Soil Sci. Soc. Am. J.* **1980**, *44*, 892–898. [[CrossRef](#)]
61. Pronk, P. Fluidized Bed Heat Exchangers to Prevent Fouling in Ice Slurry Systems and Industrial Crystallizers. Doctoral Thesis, Universiteit Delft, Delft, The Netherlands, 2006.
62. Chen, H.; Chen, K.; Yang, M.; Xu, P. A fractal capillary model for multiphase flow in porous media with hysteresis effect. *Int. J. Multiphas. Flow* **2020**, *125*, 103208. [[CrossRef](#)]
63. Wang, X.; Wang, X.; Wang, P.; Huo, Z.; Wang, C. The Effect of Salinity on Soil Seasonal Freezing-Thawing Process in Areas with Shallow Water Table Depth. Unpublished results. 2023.
64. DRIPD. Measuring Soil Salinity. Available online: <https://www.agric.wa.gov.au/soil-salinity/measuring-soil-salinity> (accessed on 9 January 2023).
65. Meter. Measurement Volume of Meter Volumetric Water Content Sensors. Available online: <https://www.metergroup.com/en/meter-environment> (accessed on 15 January 2023).
66. Wang, X. Monitoring and Simulation of Water, Heat and Salt Process under Freezing-Thawing Conditions in Saline Soil. Doctoral Thesis, China Agricultural University: Beijing, China, 2021.
67. Liu, G.; Wang, C.; Wang, X.; Huo, Z.; Liu, J. Growing season water and salt migration between abandoned lands and adjacent croplands in arid and semi-arid irrigation areas in shallow water table environments. *Agric. Water Manag.* **2022**, *274*, 107968. [[CrossRef](#)]
68. Tian, Z.; Wang, L.; Ren, T. Measuring soil freezing characteristic curve with thermo-time domain reflectometry. *Eur. J. Soil Sci.* **2023**, *74*, e13335. [[CrossRef](#)]

Disclaimer/Publisher’s Note: The statements, opinions and data contained in all publications are solely those of the individual author(s) and contributor(s) and not of MDPI and/or the editor(s). MDPI and/or the editor(s) disclaim responsibility for any injury to people or property resulting from any ideas, methods, instructions or products referred to in the content.